Influence of functional groups on toxicity of carbon nanomaterials

Yongchun Liu [1, 2], Haotian Jiang [2, 4], Chunmei Liu [3], Yanli Ge [2], Lian Wang [2], Bo Zhang [2], Hong He [2, 4,5], Sijin Liu [2, 4]

[1] Aerosol and Haze Laboratory, Advanced Innovation Center for Soft Matter Science and Engineering, Beijing University of Chemical Technology, Beijing, 100029, China

[2] State Key Joint Laboratory of Environment Simulation and Pollution Control, Research Center for Eco-Environmental Sciences, Chinese Academy of Sciences, Beijing, 100085, China

[3] Bioduro Technology (Beijing) Co., Ltd., Beijing, 102200, China

[4] University of Chinese Academy of Sciences, Beijing, 100049, China

[5] Center for Excellence in Urban Atmospheric Environment, Institute of Urban Environment, Chinese Academy of Sciences, Xiamen 361021, China.

Correspondence to: Y. Liu (liuyc@buct.edu.cn) and S. Liu (sjliu@rcees.ac.cn)

Abstract:

It has been well recognized that carbon nanomaterials and soot particles are toxic for human health, while it is still controversial about the influence of functionalization on their toxicity as well as the evolution of the toxicity of carbon nanomaterials due to chemical aging in the atmosphere. In the current study, the oxidation potential measured by dithiothreitol (DTT) decay rate and the cytotoxicity to murine macrophage cells of different functionalized carbon nanomaterials were investigated to understand the role of functionalization in their toxicities. The DTT decay rates of special black 4A (SB4A), graphene, graphene oxide, single wall carbon nanotubes (SWCNT), SWCNT-OH and SWCNT-COOH were 45.9±3.0, 58.5±6.6, 160.7±21.7, 38.9±8.9, 57.0±7.2 and

36.7±0.2 pmol $min^{-1}\mu g^{-1}$, respectively. Epoxide was found to be mainly responsible for the largest DTT decay rate of graphene oxide compared with other carbon nanomaterials based on comprehensive characterizations. Both carboxylation and hydroxylation showed little influence on the oxidation potential of carbon nanomaterials, while epoxidation contributes to the enhancement of oxidation potential. All these carbon nanomaterials were toxic to murine J774 cell line. However, oxidized carbon nanomaterials (graphene oxide, SWCNT-OH and SWCNT-COOH) showed weaker cytotoxicity to J774 cell line compared with the corresponding control sample as far as the metabolic activity was considered and stronger cytotoxicity to J774 cell line regarding to the membrane integrity and DNA incorporation. These results imply that epoxidation might enhance the oxidation potential of carbon nanomaterials.

1. Introduction

Carbon nanomaterials are predominantly composed of carbon atoms, only one kind of element, but they have largely diverse structures characterized by different degrees of crystallinity and different macro- and micromorphology (Somiya, 2013). Their basic structure is that of graphite with planes of honeycomb-arranged carbon atoms. Carbon black (CB), which is produced from incomplete combustion of heavy petroleum materials under controlled conditions (Apicella et al., 2003), has been widely used in industrial products, such as inkjet printer ink, rubber and plastic products (Lee et al., 2016), electrically conductive plastics (Parant et al., 2017), paints, coatings and cosmetics (Sanders and Peeten, 2011) and so on. CB is a quasi-graphitic form of nearly pure element carbon (EC, consist of graphene layers). It is distinguished by its very low quantities of extractable organic compounds and total inorganics (Long et al., 2013) compared with soot or black carbon (BC) (Andreae and Gelencser, 2006). Soot or BC, which originates from incomplete combustion of biomasses, biofuels, fossil fuels and natural fires in reduced or anoxic environments, is a mixture of elemental carbon and organic carbon (OC) compounds (Muckenhuber and Grothe, 2006). In addition, as a class of engineering nanoparticles, carbon nanotubes (CNTs) and graphene materials are also a large group of carbon nanomaterials although their graphene sheets are arranged more regularly (Hu et al., 2010) than that in CB (Nienow and Roberts, 2006). During production and use of these consumer products, they are prone to enter into the environment and ultimately the human body (Helland et al., 2007;Tiwari and Marr, 2010), subsequently, to pose risk of adverse health effect.

The adverse effect of CB and soot particles on human health has attracted much attention in the atmospheric chemistry community (Baumgartner et al., 2014). Overall, exposure to CB is associated with high risk of cancer, respiratory and cardiovascular diseases (WHO, 2013;Niranjan and Thakur, 2017). Mitochondrial damage in alveolar macrophages and bronchial epithelial cells resulted from exposure of diesel exhaust particles (DEPs) has been observed (Li et al., 2002a;Li et al., 2002b). Oxidation stress or reactive oxygen generation (ROS) is one of mechanisms related to the toxicity of particles including soot particles (Nel et al., 2006), and has been even used as a paradigm to assess particle toxicity (Xia et al., 2006).

Dithiothreitol (DTT) decay rate is commonly used as a cell-free measure of the oxidative potential of different particles (Cho et al., 2005;Charrier and Anastasio, 2012;Kumagai et al., 2002), such as ambient particles (Li et al., 2003;Fang et al., 2016;Cho et al., 2005;Charrier and Anastasio, 2012;Wang et al., 2013), secondary organic aerosol (SOA) (McWhinney et al., 2013b), DEP (Li et al., 2009;McWhinney et al., 2013a), carbon nanotubes (CNT)(Liu et al., 2015), flame soot (Antinolo et al., 2015;Holder et al., 2012;Li et al., 2013) and commercial carbon black (CB) particles (Koike and Kobayashi, 2006;Li et al., 2009;Li et al., 2015;Li et al., 2013). However, the reported DTT decay rate of soot and CB particles varied substantially, from 0.9 to ~50 pmol min^{-1} μg^{-1}. The variation of DTT decay rate among different samples implies the importance of the composition or structure of particles in their toxicities.

Although transition metals, element carbon, humic-like substances and quinones are responsible for ROS generation on particle surface (McWhinney et al., 2013b;Li et

al., 2003), more work is still required to deeply understand the toxicity of soot and the reason why the toxicity varies greatly among different soot samples. On the other hand, soot particles are prone to undergo oxidation by O_3, OH and NOx etc. during transport in the atmosphere. Subsequently, functionalization including formation of OH, C=O, epoxide (C-O-C) and COOH occurs (Mawhinney et al., 2000;Liu et al., 2015;Holder et al., 2012;Corbin et al., 2015). This make it more complicate to understand the toxicity of soot particles. For example, several studies have found that atmospheric relevant oxidation of CB or BC by O_3 leads to enhancement of their oxidative potential (Li et al., 2009;Li et al., 2013;Li et al., 2015;Antinolo et al., 2015;Holder et al., 2012). In particular, the DTT decay rate of soot particles has been found increasing as a function of the content of quinone formed via ozone oxidation of organic carbons in soot (Antinolo et al., 2015). However, some other studies have found that oxidation of CB or soot by O_3 or OH under atmospheric related conditions has little influence on their oxidative potential or cytotoxicity although surface functionalization is observable (Liu et al., 2015;Peebles et al., 2011). Therefore, it is necessary to understand the role of functional groups in the toxicity of soot and CB particles.

During combustion process, however, multiple functional groups including OH, C=O, COOH, esters and so on are usually formed at the same time and present in both OC and EC (Han et al., 2012a). Thus, it is difficult to differentiate the role of one kind of functional group from others in the toxicity of soot particles. Carbon black (CB), which is produced from incomplete combustion of heavy petroleum materials under controlled conditions (Apicella et al., 2003), and engineered carbon nanomaterials are

a quasi-graphitic form of nearly pure element carbon (EC, consist of graphene layers) and are distinguished by its very low quantities of extractable organic compounds and total inorganics (Long et al., 2013) compared with soot. Therefore, it is possible to investigate the role of functional groups in the toxicity of carbon nanomaterials when using CB or engineered carbon particles with different functional groups as model sample of soot particles. Actually, it has been recognized that the surface properties of carbon nanomaterials will influence their biological effects or toxicity (Lara-Martinez et al., 2017;Liu et al., 2014b;Koromilas et al., 2014). For example, a recent study has found that hydrated graphene oxide exhibited a higher cytotoxicity to THP-1 and BEAS-2B cells as a consequence of lipid peroxidation of the surface membrane and membrane lysis compared to pristine and reduced graphene oxide (Li et al., 2018). Functionalized multiwalled carbon nanotubes (FMWCNTs) is highly cardioembryotoxic in comparison with functionalized oxygen-doped multiwalled carbon nanotubes (Lara-Martinez et al., 2017). As pointed out by Lara-Martinez et al. (2017), however, cytotoxic effects of carbon nanomaterials at the cellular level generate considerable controversy and more research is clearly needed to gain insight into the mechanism of these adverse effects. In addition, passive diffusion and energy-dependent endocytosis are the two methods suggested for particles entry into living cells (Foroozandeh and Aziz, 2018). They can also be distributed to various parts of the body, from where they can either remain, translocate, or be excreted. Therefore, it is meaningful to investigate the influence of functionalization on other endpoints alone even for these carbon nanomaterials.

In the current study, both the cell-free toxicity and the cell cytotoxicity of carbon nanomaterials with different functionalities were evaluated to focus on the role of functionalization in their toxicities. DTT decay rate representing the oxidative potential and the cytotoxicity of murine macrophage cell were investigated. The carbon nanomaterials were characterized with inductively coupled plasma-mass spectrometry (ICP-MS), thermal gravity analysis (TGA), X-ray photoelectron spectroscopy (XPS), transmission electron microscopy (TEM) and zeta potential analyzer. The role of oxygen containing species in the toxicity of carbon nanomaterials was discussed. This work will be helpful for understanding the toxicity of carbon nanomaterials with different functional groups.

2. Experimental Section

2.1 Chemicals and characterization of particle samples. Commercial carbon nanomaterials including Special Black 4A (SB4A), graphene, graphene oxide, SWCNT, SWCNT-OH and SWCNT-COOH were used in this study. All these functional groups have been identified in soot particles and chemical aged soot or CB particles. SB4A was supplied by Degussa. The other carbon nanomaterials with purity >98% were supplied by Timesnano. To obtain graphene oxide with low epoxide content, graphene oxide was thermally treated at 200 °C for 30 min in high purity (99.999%) nitrogen flow. Dithiothreitol (DTT) was supplied by Sigma-Aldrich. 5,5′-dithiobis-(2-nitrobenzoic acid) (DTNB) was obtained from Alfa Aesar. Standard solutions of metal ions including Cr, Mn, Fe, Co, Ni, Cu, Zn, Cd, As, Sn and Pb were supplied by National Institute of Metrology, China. 30 % H_2O_2 solution was supplied by Sinopharm

145 Chemical Reagent Co., Ltd.

146 A transmission electron microscope (H-7500, Hitachi) was used to investigate the
147 morphologies of carbon nanomaterials. Particles were ultrasonically dispersed in
148 ultrapure water (18 MΩ) and a droplet of suspending liquid was deposited onto a Cu
149 microgrid. An acceleration voltage of 80 kV was used for measurements. The
150 morphologies were shown in Fig. S1. The diameter of primary particles were analyzed
151 by ImageJ 1.41 software (Liu et al., 2010). The diameter of the primary carbon sphere
152 for SB4A was 66±17 nm SB4A. The out diameter (OD) of SWCNT, SWCNT-OH and
153 SWCNT-COOH was <2 nm with fiber length of 1-3 μm according to the product report
154 and also confirmed by TEM (Fig. S1). Graphene and graphene oxide were 2-
155 dimensional materials with monolayer and the diameter of 0.5-3 μm.

156 XPS were measured using an AXIS Supra/Ultra (Kratos, Kratos Analytical Ltd.) to
157 identify the oxygen containing species on the surface of carbon nanomaterials. The
158 samples were excited by Al Kα X-ray ($h\nu$=1486.7 eV) with 15 kV of working voltage
159 and 40 mA of emission current. The spectra were analyzed with XPS Peak software.
160 The content of organic carbon (OC) in carbon nanomaterials was measured by thermal
161 desorption using a commercial TG instrument (TGA/DSC1/HT1600, Mettler-Toledo
162 Co., Ltd.). The amount of OC lost from the particles was recorded when the temperature
163 was ramped from 30 to 300 °C at 10 °C min^{-1} in nitrogen flow according to the protocol
164 reported in previous work (Han et al., 2012a). Metals in the particles were measured
165 with an inductively coupled plasma mass spectrometer (ICP-MS 7500a, Agilent
166 Technologies) after digested with concentrated 1:3 HNO_3/HCl. Transition metals were

quantified with the standard solution. Zeta potentials of the carbon nanomaterials were measured after sonicating for 30 min in ultrapure water (18.2 MΩ) by using a Nanoparticle Size & Zeta Potential Analyzer (Zetasizer Nano, ZS90).

2.2 DTT assay test. The DTT assay is an indirect chemical assay used for measuring the redox cycling capacity of PM. The added DTT is oxidized to its disulfide form by the ROS in particulate matter (Kumagai et al., 2002). Thus, the rate of DTT consumption is proportional to the concentration of the ROS in the sample (Cho et al., 2005). In this study, ~150 μg carbon nanomaterials were suspended in 10.0 ml phosphate buffer (0.1 M, pH 7.4) and sonicated for 15 min. 2.0 ml of 0.5 mM DTT solution was added to 3.0 ml aliquots of the sonicated suspensions. A redox reaction took place in a thermostat shaking chamber at 37 ºC. The remained DTT concentration was measured every 15 minutes by adding 0.25 ml of the reaction mixture filtration to 1.0 ml of 0.25 mM DTNB solution. DTNB reacted with the thiol groups in DTT to form a yellow compound (2-nitro-5-thiobenzoate, NTB), which could be detected by UV-vis absorption spectrometer (723N, Shanghai Ruiting Technology Co., Ltd) at 412 nm. Then, the amount of DTT consumed by PM was calculated according to the standard curves of DTT. The loss rate of DTT via a redox reaction in the presence of PM was monitored as the decrease of DTT concentration and normalized to the particle mass. Blank experiments were carried out without carbon nanomaterial particles in the buffer solution. For some samples, the response to the DTT assay was also measured for the water-soluble components of SWCNT by filtering aliquots of the samples with a 0.22 μm syringe PTFE filter, and measuring the activity of the solution without particles.

2.3 In vitro assays. Carbon nanomaterial particles were dispersed with 0.025% Tween-80 in 0.19% NaCl solution using a Dounce glass homogenizer, followed by sonication. A homogeneous and stable suspension of SWCNTs was obtained after the sonication process. Cytotoxicity assessment of carbon nanomaterials was carried out using the murine J774 cells. Three different assays targeting distinct mechanisms of cellular metabolic perturbations were assessed simultaneously, including ATP (energy metabolism), LDH (membrane integrity) and BrdU (incorporation into DNA) assays. The experiments were carried out according to the corresponding protocol. Briefly, 4×10^5 J774 cells ml^{-1} were exposed to carbon particles in 96-well plates for 24 hours for ATP and LDH assays, while the initial J774 cell concentration was 2×10^5 cells ml^{-1} for BrdU assay. Carbon nanomaterials were dosed at 0, 10, 30 and 100 μg cm^{-2} in a final volume of 200 μl $well^{-1}$ as similar to that reported in literatures (Kumarathasan et al., 2014;Kumarathasan et al., 2012). The luminescence spectroscopy of the supernatant after centrifugal separation at 1000 rpm for 5 min was measured after 24 h of cell exposure using a Multimode Microplate Reader (Varioskan®Flash, Thermo Fisher Scientific). The zero dose of carbon nanomaterials referred to the blank experiment and also means the toxicity of 0.025% Tween-80 alone in 0.19% NaCl solution. Similar to the literature results (Hadrup et al., 2017), they did not incur any obvious deleterious effect on cells growth. In addition, it has been well recognized that carbon nano-particles tended to aggregate in water even after ultrasonic dispersion. Tween-80 has been verified to be a biocompatible dispersant for carbon black (Kim et al., 2012). Negative control experiments were performed in wells containing medium without cells

211 to obtain a value for background luminescence. Positive control experiments were
212 carried out with H_2O_2 solution for LDH assays (Fig. S2).

213 **3. Results**

214 **3.1 Oxidative potential of carbon nanomaterials.** Figure 1 shows the DTT decay
215 rates of SB4A, graphene, graphene oxide, SWCNT, SWCNT-OH and SWCNT-COOH.
216 They were 45.9±3.0, 58.5±6.6, 160.7.0±21.7, 38.9±8.9, 57.0±7.2 and 36.7±0.2 pmol
217 $min^{-1}\mu g^{-1}$, respectively. Except for graphene oxide, the measured DTT decay rates for
218 these carbon nanomaterials (with mean value of 47.4±10.1 pmol $min^{-1}\mu g^{-1}$) were
219 comparable with the DTT loss rates of BC reported in the literatures. For example, it
220 was 36.2±4.9 pmol min^{-1} μg^{-1} for Printex U (Li et al., 2015) and 59.3±7.4 pmol min^{-1}
221 μg^{-1} for SWCNT (Liu et al., 2015). These values were also comparable with that of the
222 typical soot particles (BC), such as 33.6 pmol min^{-1} μg^{-1} for methane flame soot (Holder
223 et al., 2012), 49±7 pmol min^{-1} μg^{-1} for propane flame soot (Antinolo et al., 2015), 27.0
224 pmol min^{-1} μg^{-1} for hexane flame soot (Li et al., 2013), as well as the typical ambient
225 $PM_{2.5}$ particles (34.7±19.1 pmol min^{-1} μg^{-1}) (Charrier and Anastasio, 2012;Liu et al.,
226 2014a). However, the measured DTT decay rates for these carbon nanomaterials were
227 significantly higher than that of diesel soot (6.1 pmol min^{-1} μg^{-1}) and graphite (0.9 pmol
228 min^{-1} μg^{-1}) (Li et al., 2013) reported in previous work. It should be noted that the DTT
229 decay rate of graphene oxide measured in this study was 160.7±21.7 pmol min^{-1} μg^{-1}.
230 Based on T-test, the DTT decay rate of graphene oxide was significantly higher than
231 that of other tested carbon nanomaterials at the 0.05 level (t=8.498, which is greater
232 than the critical value of 2.447). This means that graphene oxide definitely has a

stronger oxidative potential than other CB or carbon nanomaterials in this work.

3.2 Cytotoxicity of carbon nanomaterials to murine J774 cell line. At the present time, the A549 (a human adenocarcinomia alveolar epithelial cell) and THP-1 (a human leukemia monocytic cell line) cell lines were usually chosen as target cell lines (Kumarathasan et al., 2012;Kumarathasan et al., 2014;Liu et al., 2015) to evaluate the alveolar and pulmonary toxicity of CB particles. As the first barrier of the immune system, macrophage cell lines will fight against the invaded particles in the lungs. Macrophage cell lines like J774 cells are ideal model systems for establishing the biophysical foundations of autonomous deformation and motility of immune cells (Lam et al., 2009). It has been found that CB nanoparticles are able to stimulate the release of macrophage chemo-attractants when exposed to type II epithelial cell lines (L-2 cells) at sub-toxic doses (Barlow et al., 2005). CNTs exposure can also lead to biological changes in J774 cells (Kumarathasan et al., 2012). Therefore, it is meaningful to investigate the cytotoxicity of different carbon nanomaterials as well as the influence of surface functional group on the macrophage cell lines.

Figure 2 shows the in vitro toxicities of SB4A, graphene, graphene oxide, SWCNT, SWCNT-COOH and SWCNT-OH. The stars mean the indicator of the toxicity at a certain dose of carbon nanomaterials is significantly different from the corresponding blank experiments at 0.05 level. As shown in Fig. 2, the metabolic activity of J774 cell line decreased monotonously as a function of the dose of all these carbon nanomaterials. The relative ATP level (1.01±0.02) at the SB4A dose of 10 μg cm^{-2} was almost the same as that of the blank sample, while it significantly decreased to 0.89±0.05 and 0.61±0.07

when the dose of SB4A increased to 30 μg cm^{-2} and 100 μg cm^{-2}, respectively. Similarly, the relative ratio of BrdU incorporation decreased from 0.74±0.03 to 0.60±0.04 when the dose of SB4A increased from 30 to 100 μg cm^{-2}. However, the released LDH levels were constant within experiment uncertainty at different SB4A doses.

As shown in Fig. 2B-F, the metabolic activity of murine J774 cell decreased more significantly when exposed to engineered carbon nanomaterials than SB4A. For example, the relative ratio of ATP level was 0.67±0.06, 0.84±0.03, 0.59±0.10, 0.93±0.01 and 0.88±0.02 even when the J774 cells were exposed to 10 μg cm^{-2} graphene, graphene oxide, SWCNT, SWCNT-OH and SWCNT-COOH, respectively. When exposed to high doses of engineered carbon nanomaterials, the reduction of relative ATP level became more significant. These results mean the cytotoxicity of the engineered carbon nanomaterials studied in this work are stronger than that of SB4A regarding to metabolic activity. Graphene, graphene oxide and SWCNT-COOH significantly enhanced release of LDH at different exposure levels, while SWCNT and SWCNT-OH only led to significant increases of released LDH at high exposure level (100 μg cm^{-2}).

It should be noted that the reduction of ATP ratio of J774 cells exposed to graphene oxide was weaker than that of graphene. The reduction of ATP ratio of J774 cells exposed to SWCNT-OH or SWCNT-COOH was also weaker than that of SWCNT. However, compared with graphene, graphene oxide showed much stronger toxicity to J774 cell as far as the membrane integrity was considered. The released LDH at exposure level of 30 μg cm^{-2} graphene oxide was comparable with that when exposed

277 to 150 ppm H_2O_2 (Fig. S2). In addition, graphene oxide, SWCNT-OH and SWCNT-
278 COOH significantly inhibited DNA synthesis of J774 cells when the carbon
279 nanomaterials doses were above 10 μg cm^{-2}, while graphene and SWCNT did not show
280 significant inhibition of DNA synthesis for J774 cells. For instance, the relative ratio of
281 BrdU when J774 cells exposed to 100 μg cm^{-2} of graphene oxide was 0.61±0.10, while
282 it was 0.77±0.10 for graphene exposed cells at the same exposure level. They were
283 0.62±0.10 for SWCNT-OH and 0.56±0.09 for SWCNT-COOH treated cell at a dose of
284 10 μg cm^{-2} compared with 0.83±0.09 for 10 μg cm^{-2} of SWCNT treated J774 cell.
285 **3.3 Characterization of carbon nanomaterials.** As shown in Fig. S1, the
286 morphologies of these carbon nanomaterials varied greatly. SB4A was a zero-
287 dimensional material. SWCNT, SWCNT-OH and SWCNT-COOH were one
288 dimensional material. Graphene and graphene oxide were two dimensional materials.
289 The content of transition metals including Cr, Fe, Mn, Co, Ni, Cu, Zn, As, Cd, Sn
290 and Pb were measured by using an ICP-MS after the carbon nanomaterials were
291 digested with 1:3 HNO_3/HCl. As shown in Fig. S4A, Fe was the most abundant
292 transition metal in these carbon nanomaterials. Its concentration varied from 122 μg g^{-1}
293 to 6596 μg g^{-1} among different carbon nanomaterials. The concentration of other
294 metals varied from zero to several hundred μg g^{-1} depending on both carbon
295 nanomaterials and the type of metals. Compared with SB4A, these engineered carbon
296 nanomaterials showed higher metal content. For example, the total metal content in
297 graphene was 6 times as high as that in SB4A, while it was 33 times in SWCNT as high
298 as that in SB4A. This can be explained by the fact that graphene and SWCNT materials

were catalytically synthetized using metal catalysts containing Fe, Co or Ni (Maruyama, 2018).

Figure 3 shows the thermo gravity and differential thermal analysis curves for these CB materials when the temperature was ramped from 30 to 300 °C at 10 °C min^{-1} in nitrogen flow. Weight loss (Fig. 3A) accompanied with an endothermic process (Fig. 3B) were observed below 60°C for all of these samples. This can be ascribed to desorption of surface adsorbents including bonded organics and trace water. As shown in Fig. 3B, the saddle points of these differential thermal analysis curves were observed at 35, 35, 41, 42, 56 and 58 °C for graphene, SWCNT, SB4A, SWCNT-OH, SWCNT-COOH and graphene oxide, respectively. It should be noted that the oxidized carbon nanomaterials such as SWCNT-OH, SWCNT-COOH and graphene oxide showed higher saddle points of the heat curves than graphene, SWCNT and SB4A. This implies stronger interaction between the adsorbents and these three oxidized carbon nanomaterials compared with the counterpart. Therefore, it is reasonable to deduce that the adsorbed water mainly contributes to the weight loss in this stage. The sample weight slightly decreased as the temperature further increased for all of these carbon nanomaterials except for graphene oxide and accompanied with a gradual increase of the heat flow. This can be ascribed to desorption of adsorbed organics from the surface of the carbon nanomaterials. The relatively small increase rate of the heat in this stage was consistent with the small heat capacity of organics when compared with the first one which was ascribed to desorption of water. For graphene oxide, however, weight loss (from 32% to 60%) was significantly observed accompanied with an acute

exothermic process when the temperature increased from 150 to 200 °C as shown in Fig. 3B. This implies that release of pyrolysis products and structure collapse of graphene oxide occur. It also means a high reactivity of graphene oxide and highlights the distinctive property of graphene oxide among these investigated carbon nanomaterials. The adsorbed organics were estimated based on the thermogravimetric curves when the possible contribution of water was ruled out. For graphene oxide, 150 °C was taken as the endpoint, while 300 °C was chosen for other samples. The content of adsorbed organics on SB4A, graphene, graphene oxide, SWCNT, SWCNT-OH and SWCNT-COOH was 6 %, 13 %, 15 %, 9 %, 5 % and 9 %, respectively.

To further investigate the role of surface oxygen in the toxicity of carbon nanomaterials, the oxygen-containing species of these carbon nanomaterials were identified with X-ray photoelectron spectroscopy. Fig. 4 shows the typical O1s and C1s spectra of these carbon nanomaterials. Several oxygen-containing species were observed as shown in Fig. 4A-F. Adsorbed oxygen was observed at 535.2 eV in the O1s spectra. Carbon-oxygen single bond in hydroxyl group (C-OH) and epoxide (C-O-C) were at 533.5 and 532.6 eV, respectively. Carbon-oxygen double bound (C=O) was observed at 531.8 eV, while highly conjugated form of carbonyl oxygen such as quinone groups was identified at 530.5 eV (Schuster et al., 2011). In the C1s spectra (Fig. 4G-L), the band at 291 eV was attributed to the shakeup peak associated with π-π* transition (Simmons et al., 2006). The band at 289 eV corresponded to carbonyls and epoxides was observed at 287 eV (Kuznetsova et al., 2001). The band at 285 eV and 284.6 eV was assigned to graphite and sp^3 carbon, respectively. In particular, the

intensity of C-O-C at 532.6 eV in graphene oxide was very strong compared with other carbon nanomaterials. At the same time, the band of C-O-C at 287 eV was also much stronger than that of other carbon nanomaterials in the C1s spectrum. These results mean that epoxides (C-O-C) is the predominating species (Fig. 5C and I) in graphene oxide.

4. Discussion

As shown in Fig. 2, all the carbon nanomaterials showed decreased ATP activities as a function of the dose. This means the carbon nanomaterials investigated in this work are toxic to murine J774 cell line. This is consistent with the previous results that CNT and Printex U are toxic to J774 cells (Kumarathasan et al., 2012) and graphene oxide can induce dose-dependent cell death in normal lung fibroblasts (HLF), macrophages (THP-1 and J744A), epithelial (BEAS-2B) cells, lung cancer cells (A549) etc. (Zhang et al., 2016;Li et al., 2018). At the same time, the BrdU activities decreased as a function of the dose of carbon nanomaterials, which means they are inhibitor for cell proliferation of murine J744 (Cappella et al., 2015). In addition, except for SB4A, other carbon nanomaterials showed significant increases in LDH. This means that the integrity of cell membrane decreased when J774 cells were exposed to these engineered carbon nanomaterials, while the cell membrane might be intact when exposed to SB4A (Cho et al., 2008;Kumarathasan et al., 2015). This might be related to lipid peroxidation induced by these engineered particles (Li et al., 2018) and the non-sphere feature of these engineered particles as observed in Fig.S1. These results also consistent with the previous study that observed CNT cytotoxicity ranking was assay-dependent

365 (Kumarathasan et al., 2015).

366 As shown in Fig. S3, all these carbon nanomaterials revealed negative zeta potential
367 from -42 mV to -20 mV. SB4A, graphene oxide and SWCNT-COOH almost borne the
368 same zeta potential (-42 mV), while SWCNT, SWCNT-OH and graphene showed
369 comparable zeta potential. This observation suggested the stability of dispersed SB4A,
370 graphene oxide and SWCNT-COOH in water and the interaction between these
371 particles with cells was comparable. However, the cytotoxicity of SB4A, graphene and
372 SWCNT showed an increase trend regarding the metabolic activity of J774 cell (Fig.
373 2). This can be explained by the different mode of action (MOA) when the cells were
374 exposed to different types of nanomaterials. For example, adhesions and/or covering
375 on cells could be the main MOA for graphene/graphene oxide (2-D structure) (Gupta
376 et al., 2019;Keshavan et al., 2017), while for carbon nanotubes (1-D structure), piercing
377 and/or internalization by cells could be the main MOA (Lacerda et al., 2013). This
378 means morphology should plays a role in determining the cytotoxicity of the carbon
379 nanomaterials studied in this work. Therefore, in the following section we mainly
380 discuss the cytotoxicity among these materials having same dimension, such as
381 SWCNT-OH and SWCNT-COOH verse SWCNT and graphene oxide verse graphene.

382 It should be noted that oxidized carbon nanomaterials including graphene oxide,
383 SWCNT-OH and SWCNT-COOH showed weaker reduction of ATP ratio of J774 cells
384 than the counterparts (Fig. 2). These results suggested that functionalized carbon
385 nanomaterials caused a low cytotoxicity of murine J774 cell line regarding to the cell
386 apoptosis, while a stronger toxicity was demonstrated for cell proliferation and the

membrane integrity. This finding was true, in particular, for graphene oxide. However, we did not observe a clear dependence of cytotoxicity to murine J774 cell line on the morphology, the transition metal content, the OC content and the content of oxygen-containing species on the surface of carbon nanomaterials although oxidized CB materials showed reduced toxicity to J774 cell lines as far as metabolic activity was considered. In particular, the difference in surface oxygen content between graphene oxide and graphene was much higher than that between SWCNT-OH/SWCNT-COOH and SWCNT (Fig. 5A), while the differences in metabolic activity to J774 cell line between graphene oxide and graphene was similar to that between SWCNT-OH/SWCNT-COOH and SWCNT. The pathways of cellular toxicity induced by particles reside in both oxidative stress (ROS) and non-oxidative stress dependent (Shvedova et al., 2012). Oxidative stress leads to selective oxidation of mitochondrial CL, NADPH oxidase activation and MPO activation in neutrophils, while non-oxidative stress results from interference with mitotic spindle and actin cytoskeleton, and steric hindrance of ion channels. The interaction between target cells and particles should be much complicated than that between DTT and particles. As discussed above, the cytotoxicity of nano-particles relied on not only the mode of action but also the chemical nature of particles. Therefore, the different responses of the oxidation potential and the cytotoxicity to the epoxide content in these carbon materials might be accounted for by different mechanisms of toxicity among these assays.

The DTT decay rate (Fig. 1) did not show obvious dependence on their morphologies in this work. For example, except for graphene oxide, the DTT decay

409 rates were comparable among all the other materials regardless of the morphology.
410 Graphene and graphene oxide showed similar particle size, graphene layer and
411 morphologies (Fig. S1), while they showed totally different toxicity as shown in Fig. 1.
412 Transition metals in the particles have been identified to be the important contributor
413 to ROS generation (McWhinney et al., 2013b;Li et al., 2003). It should be noted that
414 although the metal content of SB4A was very low compared with other materials (Fig.
415 S4), the DTT decay rate of SB4A was still comparable with these engineered carbon
416 nanomaterials except for graphene oxide as shown in Fig. 1. On the other hand,
417 SWCNT had the highest metal content, while graphene oxide rather than SWCNT
418 showed the strongest DTT decay rate. In addition, the soluble metal contents were in
419 the following order: SWCNT-COOH > SWCNT > SB4A > graphene oxide > graphene >
420 SWCNT-OH (Fig. S4B), after being sonicated for 30 min in water. Graphene oxide
421 (103.7 μg g^{-1}) did not show a significant difference compared with SB4A (106.3 μg g^{-1})
422 and graphene (93.7μg g^{-1}). These results indicated that the high oxidative potential of
423 graphene oxide relative to other materials cannot be attributed to their difference in
424 bounded or soluble transition metals. This can be explained by the following reasons.
425 First, metal content was measured after digested with 1:3 HNO_3/HCl. The speciation of
426 metals should be quite different from that presenting in the pristine carbon
427 nanomaterials. For example, the contents of soluble metal ions after sonicated for 30
428 min (Fig. S4B) varied from zero to 356 μg g^{-1}. These values were much lower than the
429 corresponding metal contents of digested samples as shown in Fig. S4A. Second, metal
430 might be in the inner pores of carbon nanomaterials. This will decrease the efficiency

of metals to generate ROS. Finally, the concentration of carbon nanomaterials was 10-40 μg ml^{-1} in DTT assay tests. This meant the concentration of transition metals was at ng ml^{-1} level even if all of the transition metals were available. The low concentration of metals released might lead to negligible contribution to ROS formation. This was further confirmed by the very small DTT decay rate of the SWCNT filtered solution (1.66±0.15 pmol min^{-1} μg^{-1}) compared with that of SWCNT suspension (38.9±8.9 pmol min^{-1} μg^{-1}) even though SWCNT had the highest metal concentration (Fig. S4A). This was consistent with the previous conclusions that redox activity originates from the particle surface of CB or BC materials but not from water-soluble substances (Liu et al., 2015;McWhinney et al., 2013a).

As shown in the insert graph of Fig. 3A, the content of organics cannot explain the sequence of the DTT loss rate (Fig. 1) of these carbon nanomaterials. For example, the content of organics on graphene and graphene oxide were almost the same, while the DTT decay rate of graphene oxide was as about 2.5 times as that of graphene (Fig. 1) This means the different DTT loss rate observed in this study cannot be explained by the adsorbed organics among these materials.Fig. 5A summarizes the distribution of the oxygen species mentioned above normalized to O atoms in these carbon nanomaterials. Highly conjugated form of carbonyl oxygen (quinone) and adsorbed oxygen contributed little to the total oxygen on the surface (<1 %), while C=O, C-O-C and C-OH were predominating oxygen-containing species. Our results agree well with the previous work that C=O, C-O-C and C-OH dominated oxygen-containing species on natural chars, diesel soot, hexane soot and activated charcoal (Langley et al., 2006).

453 Although quinone has been well recognized to contribute to ROS generation on the
454 surface of fine particles (Kumagai et al., 2002;Li et al., 2002b), the content of quinone
455 was lower than 0.35% and showed little difference among all of these tested carbon
456 nanomaterials (Fig. 5A and B). It did so for adsorbed oxygen content. Therefore, we
457 can conclude that the very large DTT decay rates of graphene oxide compared with
458 other carbon nanomaterials as shown in Fig. 5C cannot be explained by the content of
459 quinone or adsorbed oxygen.

460 As shown in Fig. 5A, the total oxygen content of SB4A, graphene, SWCNT,
461 SWCNT-OH and SWCNT-COOH was 6.68%, 2.41 %, 2.88%, 3.60% and 9.21%,
462 respectively. They were comparable with that of diesel soot (2.1%-12.2%) (Schuster et
463 al., 2011). However, the oxygen content of graphene oxide (29.0%) was significantly
464 higher than the other carbon nanomaterials (Fig. 5A). At the same time, the distribution
465 pattern of the surface species on graphene oxide was quite different from the other
466 carbon nanomaterials. Fig. 5B compared the content of the oxygen-containing species
467 of graphene oxide with other carbon nanomaterials. The red stars indicate the content
468 of oxygen-containing species in graphene oxide, while the blue boxes show that of other
469 carbon nanomaterials. It can be seen that the content of quinone and adsorbed oxygen
470 showed no difference between graphene oxide and other carbon nanomaterials. The
471 concentration of C=O and C-OH in graphene oxide was slightly higher than that in the
472 other carbon nanomaterials. However, the content of epoxide in graphene oxide was
473 significantly higher than the other carbon nanomaterials. The content of epoxide in
474 graphene oxide normalized to O atoms was 20.8 %, which was 71.7 % of its total

475 oxygen content (Fig. 5B), while it was less than 2.7 % in other carbon nanomaterials.
476 This well corresponded to the large DTT decay rates of graphene oxide (160.7 pmol
477 min^{-1} μg^{-1}) compared to other carbon nanomaterials (less than 60 pmol min^{-1} μg^{-1}) as
478 shown in Fig. 5C. It should be noted that the content of epoxide was not linearly
479 correlated to the DTT activity. This can be explained by the typical nonlinear
480 relationship between the dose of toxicant and toxicity (Antinolo et al., 2015). It should
481 be pointed out that multiple parameters of particle may have influence on its toxicity,
482 in particular, on the cytotoxicity. For example, particle size and morphology may have
483 influence on the material mobility and uptake by cells. Although the observed toxicity
484 including DTT activity and cytotoxicity could be a coincidence of the chemical
485 composition, functional groups and morphology of these particles, the above results at
486 least imply that these physiochemical properties such as morphology, metal and OC
487 content should not be crucial factors as for the toxicity of these carbon nanomaterials
488 because it is difficult to observe an obvious dependence of the toxicity on these factors.
489 In the meantime, we can propose that epoxides in graphene oxide are mainly
490 responsible for the high ROS activity of graphene oxide. The high ROS formation
491 potential of graphene oxide might also explain its strong cytotoxicity to J774 cell line
492 regarding to the cell membrane.

493 To further confirm this assumption, we measured the ROS activity of the thermally
494 treated graphene oxide at 200 °C in nitrogen flow because the C-O-C (epoxide)
495 structure can be broken under this condition as shown in Fig. 3 and discussed above.
496 XPS spectra confirmed the broken of epoxide by the fact that the content of epoxide in

thermally treated graphene oxide decreased to 4.3% from 20.9% in graphene oxide as shown in Figs. S5 and S6. In addition, TEM results also showed that graphene oxide broke into small sheets, whose morphology and particle size were close to that of SB4A and graphene oxide or graphene (Fig. S1). At the same time, the DTT decay rate of the thermally treated graphene oxide decreased to 54.9±9.8 pmol min^{-1} μg^{-1} (Fig. 6). This value was comparable to the DTT decay rates of other carbon nanomaterials, in particular, graphene (58.5±6.6 pmol min^{-1} μg^{-1}) (Fig. 1), while it was significantly lower than the graphene oxide (160.7.0±21.7 pmol min^{-1} μg^{-1}) as shown in Fig. 6. It should be noted the total oxygen contents of thermally treated graphene oxide was 19.3 %, which was lower than that of graphene oxide (29.0 %) but significantly higher than that of other carbon nanomaterials. However, the DTT decay rate of thermally treated graphene oxide was still comparable with other carbon nanomaterials. This further highlights the importance of functional group in the DTT decay rate. Therefore, it means that epoxides in graphene oxide are the highly reactive site for ROS formation on the surface of graphene oxide. This is for the first time to observe that epoxide is a highly reactive site for ROS formation besides quinone on carbon nanomaterials. This result is also well consistent with the previous founding that epoxides in graphene oxide can oxidize SO_2 to sulfate (He and He, 2016). Recently, environmentally persistent free radicals (EPFRs) (a kind of surface stabilized metal-radical complexes characterized by an oxygen-centered radical) (Dugas et al., 2016) have been identified in different source of particles including biomass/coal combustion, diesel and gasoline exhaust, ambient $PM_{2.5}$ and polymer (Balakrishna et al., 2009;Truong et al., 2010;Dugas et al., 2016).

519 However, it is unclear that whether epoxide in graphene oxide observed in this study
520 contributes to the EPFRs formation. This is needed to be investigated in the future.

521 **5. Conclusion and atmospheric implications**

522 Oxidation is a useful method to obtain functionalized CB materials with distinctive
523 performance in industry. This process unusually leads to formation of carbonyls,
524 hydroxyls, carboxylic acids, esters, ethers and epoxides on the surface of CB or BC
525 particles. Previous work have found that oxidation of carbon nanomaterials (SWCNT)
526 by O_3 or OH under atmospheric related conditions has little influence on their oxidative
527 potential or cytotoxicity although carbonyls, carboxylic acids and esters were formed
528 (Liu et al., 2015). Similarly, surface functionalization was observed for commercial CB
529 materials by ozone oxidation, while increase in the cytotoxicity of murine macrophages
530 and release of inflammation markers upon exposure to the oxidized CB were not
531 observed (Peebles et al., 2011). However, some other studies observed that oxidation
532 process enhanced the oxidation potential (Li et al., 2015;Li et al., 2013;Antinolo et al.,
533 2015) as well as the cytotoxicity (Holder et al., 2012) of CB and BC particles. Using
534 the model carbon nanomaterials with different dominate surface functionalities in this
535 work, we have found that hydroxyl and carboxyl functionalized CB particles had little
536 influence on their oxidation potential, while epoxide functionalized CB (graphene
537 oxide) led to a very strong oxidation potential. Epoxide has been identified as a surface
538 product on SWCNT when treated with high concentration of ozone (Mawhinney et al.,
539 2000;Yim and Johnson, 2009). Besides carboxylic acids, esters (Liu et al., 2015),
540 ketone, lactone and anhydride species (Liu et al., 2010;Han et al., 2012b), epoxides has

541 also been identified as the surface product during oxidation of SWCNT in atmosphere
542 relevant conditions (Liu et al., 2015). On the other hand, graphene oxide was an
543 important commercial product, while showed strong oxidation potential as observed in
544 this work. This means that exposure to epoxide-containing carbon materials should lead
545 to high health risk regarding to oxidation potential. Therefore, Mussel-inspired
546 chemistry is necessary for fabrication of functional materials and decreasing their
547 toxicity and for biomedical applications (Liu et al., 2014b;Zhang et al., 2012).

548 It has been found that CB particles (Printex 90) can induce opening of plasma
549 membrane calcium channels leading to a calcium influx and cause significant release
550 of proinflammatory cytokine TNF-α by the murine J774 cells (Brown et al., 2004),
551 subsequently potentially induce migration of macrophages (Barlow et al., 2005). This
552 could initiate the recruitment of inflammatory cells to sites of particle deposition and
553 the subsequent removal of the particles by macrophages. The metabolic activity of these
554 hydroxyl, carboxylic acid and epoxide functionalized carbon nanomaterials increased
555 when compared with the corresponding sample as observed in this work. This implies
556 functionalization of carbon nanomaterials might not pose an enhanced cytotoxicity risk
557 to macrophages compared with the corresponding control materials although the
558 oxidized carbon nanomaterials were still toxic as far as metabolic activity was
559 considered. However, the oxidized carbon nanomaterials might pose enhanced
560 cytotoxicity to macrophages regarding to membrane integrity and DNA synthesis. It
561 should be pointed out that exposure experiments were performed under high particle
562 concentration with short exposure time in this work. More work needs to be done at

low particle concentration with long exposure time in the future. On the other hand, the interaction between particles and biological entities such as proteins or cells has not been considered in this work. Therefore, the in vivo toxicological effect of these functionalized particles needs to be further evaluated in the future.

Data availability. The experimental data are available upon request to the corresponding authors.

Supplement. The supplement related to this article is available online at:

AUTHOR INFORMATION

Author contributions. YL, HH and SL designed the experiments. YL wrote the paper. YL, HJ and YG did the DTT assay tests. CL and LW did the cytotoxicity assessments. HJ and BZ performed the characterization of samples.

ACKNOWLEDGMENTS

This research was financially supported by the National Natural Science Foundation of China (91543109 and 48177306) and the Fundamental Research Funds for the Central Universities (PT1907). YCL should thank Beijing University of Chemical Technology for financial supporting.

References:

Andreae, M. O., and Gelencser, A.: Black carbon or brown carbon? The nature of light-absorbing carbonaceous aerosols, Atmos. Chem. Phys., 6, 3131-3148, doi: 10.5194/acp-6-3131-2006, 2006.

586 Antinolo, M., Willis, M. D., Zhou, S., and Abbatt, J. P. D.: Connecting the oxidation of soot to its redox
587 cycling abilities, Nat. Commun., 6, 10.1038/ncomms7812, 2015.
588 Apicella, B., Barbella, R., Ciajolo, A., and Tregrossi, A.: Comparative analysis of the structure of carbon
589 materials relevant in combustion, Chemosphere, 51, 1063-1069, http://dx.doi.org/10.1016/S0045-
590 6535(02)00715-4, 2003.
591 Balakrishna, S., Lomnicki, S., McAvey, K. M., Cole, R. B., Dellinger, B., and Cormier, S. A.:
592 Environmentally persistent free radicals amplify ultrafine particle mediated cellular oxidative stress and
593 cytotoxicity, Part. Fibre Toxicol., 6, 10.1186/1743-8977-6-11, 2009.
594 Barlow, P. G., Clouter-Baker, A., Donaldson, K., MacCallum, J., and Stone, V.: Carbon black
595 nanoparticles induce type II epithelial cells to release chemotaxins for alveolar macrophages, Part. Fibre
596 Toxicol., 2, 11, 10.1186/1743-8977-2-11, 2005.
597 Baumgartner, J., Zhang, Y., Schauer, J. J., Huang, W., Wang, Y., and Ezzati, M.: Highway proximity and
598 black carbon from cookstoves as a risk factor for higher blood pressure in rural China, Proc. Natl. Acad.
599 Sci. USA., 111, 13229-13234, 10.1073/pnas.1317176111, 2014.
600 Brown, D. M., Donaldson, K., and Stone, V.: Effects of PM10 in human peripheral blood monocytes and
601 J774 macrophages, Resp. Res. 5, doi:10.1186/1465-9921-5-29, 2004.
602 Cappella, P., Gasparri, F., Pulici, M., and Moll, J.: Cell proliferation method: Click chemistry based on
603 brdu coupling for multiplex antibody staining, Curr. Protoc. Cy., 72, 7.34.31-17,
604 10.1002/0471142956.cy0734s72, 2015.
605 Charrier, J. G., and Anastasio, C.: On dithiothreitol (DTT) as a measure of oxidative potential for ambient
606 particles: evidence for the importance of soluble transition metals, Atmos. Chem. Phys., 12, 9321-9333,
607 10.5194/acp-12-9321-2012, 2012.
608 Cho, A. K., Sioutas, C., Miguel, A. H., Kumagai, Y., Schmitz, D. A., Singh, M., Eiguren-Fernandez, A.,
609 and Froines, J. R.: Redox activity of airborne particulate matter at different sites in the Los Angeles Basin,
610 Environ. Res., 99, 40-47, http://dx.doi.org/10.1016/j.envres.2005.01.003, 2005.
611 Cho, M.-H., Niles, A., uili Huang, Inglese, J., Austin, C. P., Riss, T., and Xia, M.: A bioluminescent
612 cytotoxicity assay for assessment of membrane integrity using a proteolytic biomarker, Toxicol. Vitro.,
613 22, 1099-1106, 2008.
614 Corbin, J. C., Lohmann, U., Sierau, B., Keller, A., Burtscher, H., and Mensah, A. A.: Black carbon surface
615 oxidation and organic composition of beech-wood soot aerosols, Atmos. Chem. Phys., 15, 11885-11907,
616 10.5194/acp-15-11885-2015, 2015.
617 Dugas, T. R., Lomnicki, S., Cormier, S. A., Dellinger, B., and Reams, M.: Addressing emerging risks:
618 Scientific and regulatory challenges associated with environmentally persistent free radicals, *Inter. J.*
619 *Env. Res. Pub. Heal.*, 13, 17, 10.3390/ijerph13060573, 2016.
620 Fang, T., Verma, V., Bates, J. T., Abrams, J., Klein, M., Strickland, M. J., Sarnat, S. E., Chang, H. H.,
621 Mulholland, J. A., Tolbert, P. E., Russell, A. G., and Weber, R. J.: Oxidative potential of ambient water-
622 soluble PM2.5 in the southeastern United States: contrasts in sources and health associations between
623 ascorbic acid (AA) and dithiothreitol (DTT) assays, Atmos. Chem. Phys., 16, 3865-3879, 10.5194/acp-
624 16-3865-2016, 2016.
625 Foroozandeh, P., and Aziz, A. A.: Insight into cellular uptake and intracellular trafficking of nanoparticles,
626 Nanoscale Res. Lett., 13, 339-339, 10.1186/s11671-018-2728-6, 2018.
627 Gupta, P., Agrawal, A., Murali, K., Varshney, R., Beniwal, S., Manhas, S., Roy, P., and Lahiri, D.:
628 Differential neural cell adhesion and neurite outgrowth on carbon nanotube and graphene reinforced
629 polymeric scaffolds, Mater. Sci. Eng. C-Mater. Biol. Appl., 97, 539-551, 10.1016/j.msec.2018.12.065,

2019.
Hadrup, N., Bengtson, S., Jacobsen, N. R., Jackson, P., Nocun, M., Saber, A. T., Jensen, K. A., Wallin, H., and Vogel, U.: Influence of dispersion medium on nanomaterial-induced pulmonary inflammation and DNA strand breaks: investigation of carbon black, carbon nanotubes and three titanium dioxide nanoparticles, Mutagenesis, 32, 581-597, 10.1093/mutage/gex042, 2017.
Han, C., Liu, Y., Liu, C., Ma, J., and He, H.: Influence of combustion conditions on hydrophilic properties and microstructure of flame soot, J. Phys. Chem. A, 116, 4129-4136, 10.1021/jp301041w, 2012a.
Han, C., Liu, Y., Ma, J., and He, H.: Effect of soot microstructure on its ozonization reactivity, J. Chem. Phys., 2012 http://dx.doi.org/10.1063/1.4747190, 2012b.
He, G., and He, H.: DFT studies on the heterogeneous oxidation of SO_2 by oxygen functional groups on graphene, Phys. Chem. Chem. Phys., 18, 31691-31697, 2016.
Helland, A., Wick, P., Koehler, A., Schmid, K., and Som, C.: Reviewing the environmental and human health knowledge base of carbon nanotubes, Environ. Health. Perspect., 115, 1125-1131, 2007.
Holder, A. L., Carter, B. J., Goth–Goldstein, R., Lucas, D., and Koshland, C. P.: Increased cytotoxicity of oxidized flame soot, Atmos. Pollu. Res. , 3, 25-31, 2012.
Hu, L., Hecht, D. S., and Grüner, G.: Carbon nanotube thin films: Fabrication, properties, and applications, Chem. Rev., 110, 5790-5844, 10.1021/cr9002962, 2010.
Keshavan, S., Oropesa-Nunez, R., Diaspro, A., Canale, C., and Dante, S.: Adhesion and migration of CHO cells on micropatterned single layer graphene, 2D Mater., 4, 9, 10.1088/2053-1583/aa57e9, 2017.
Kim, H., Park, K., and Lee, M.-Y.: Biocompatible dispersion methods for carbon black, Toxicol. Res., 28, 209-216, 2012.
Koike, E., and Kobayashi, T.: Chemical and biological oxidative effects of carbon black nanoparticles, Chemosphere, 65, 946-951, http://dx.doi.org/10.1016/j.chemosphere.2006.03.078, 2006.
Koromilas, N. D., Lainioti, G. C., Gialeli, C., Barbouri, D., Kouravelou, K. B., Karamanos, N. K., Voyiatzis, G. A., and Kallitsis, J. K.: Preparation and toxicological assessment of functionalized carbon nanotube-polymer hybrids, Plos One, 9, 10.1371/journal.pone.0107029, 2014.
Kumagai, Y., Koide, S., Taguchi, K., Endo, A., Nakai, Y., Yoshikawa, T., and Shimojo, N. C.: Oxidation of proximal protein sulfhydryls by phenanthraquinone, a component of diesel exhaust particles, Chem. Res. Toxicol., , 15, 483-489, 2002.
Kumarathasan, P., Das, D., Salam, M. A., Mohottalage, S., DeSilva, N., Simard, B., and Vincent, R.: Mass spectrometry-based proteomic assessment of the in vitro toxicity of carbon nanotubes, Curr. Top. Biochem. Res., 14, 15-27, 2012.
Kumarathasan, P., Breznan, D., Das, D., Salam, M. A., Siddiqui, Y., MacKinnon-Roy, C., Guan, J., de Silva, N., Simard, B., and Vincent, R.: Cytotoxicity of carbon nanotube variants: A comparative in vitro exposure study with A549 epithelial and J774 macrophage cells, Nanotoxicology, 9, 148-161, doi:10.3109/17435390.2014.902519, 2014.
Kumarathasan, P., Breznan, D., Das, D., Salam, M. A., Siddiqui, Y., MacKinnon-Roy, C., Guan, J., de Silva, N., Simard, B., and Vincent, R.: Cytotoxicity of carbon nanotube variants: A comparative in vitro exposure study with A549 epithelial and J774 macrophage cells, Nanotoxicology, 9, 148-161, 10.3109/17435390.2014.902519, 2015.
Kuznetsova, A., Popova, I., Yates, J. T., Bronikowski, M. J., Huffman, C. B., Liu, J., Smalley, R. E., Hwu, H. H., and Chen, J. G.: Oxygen-containing functional groups on single-wall carbon nanotubes: nexafs and vibrational spectroscopic studies, J. Am. Chem. Soc., 123, 10699-10704, 10.1021/ja011021b, 2001.
Lacerda, L., Ali-Boucetta, H., Kraszewski, S., Tarek, M., Prato, M., Ramseyer, C., Kostarelos, K., and

Bianco, A.: How do functionalized carbon nanotubes land on, bind to and pierce through model and plasma membranes, Nanoscale, 5, 10242-10250, 10.1039/c3nr03184e, 2013.
Lam, J., Herant, M., Dembo, M., and Heinrich, V.: Baseline mechanical characterization of J774 macrophages, Biophys. J., 96, 248-254, 2009.
Langley, L. A., Villanueva, D. E., and Fairbrother, D. H.: Quantification of surface oxides on carbonaceous materials, Chem. Mater. , 18, 169-178, 2006.
Lara-Martinez, L. A., Masso, F., Gonzalez, E. P., Garcia-Pelaez, I., Contreras-Ramos, A., Valverde, M., Rojas, E., Cervantes-Sodi, F., and Hernandez-Gutierrez, S.: Evaluating the biological risk of functionalized multiwalled carbon nanotubes and functionalized oxygen-doped multiwalled carbon nanotubes as possible toxic, carcinogenic, and embryotoxic agents, Inter. J. Nanomedicine, 12, 7695-7707, 10.2147/ijn.s144777, 2017.
Lee, Y. S., Park, S. H., Lee, J. C., and Ha, K.: Influence of microstructure in nitrile polymer on curing characteristics and mechanical properties of carbon black-filled rubber composite for seal applications, J. Elastomer Plast., 48, 659-676, 10.1177/0095244315613621, 2016.
Li, N., Kim, S., Wang, M., Froines, J., Sioutas, C., and Nel, A.: Use of a stratified oxidative stress model to study the biological effects of ambient concentrated and diesel exhaust particulate matter, Inhal. Toxicol., 14, 459-486, 10.1080/089583701753678571, 2002a.
Li, N., Wang, M., Oberley, T. D., Sempf, J. M., and Nel, A. E.: Comparison of the pro-oxidative and proinflammatory effects of organic diesel exhaust particle chemicals in bronchial epithelial cells and macrophages, J. Immunol., 169, 4531-4541, 2002b.
Li, N., Sioutas, C., Cho, A., Schmitz, D., Misra, C., Sempf, J., Wang, M., Oberley, T., Froines, J., and Nel, A.: Ultrafine particulate pollutants induce oxidative stress and mitochondrial damage, Environ. Health Persp., 111, 455-460, 2003.
Li, Q., Wyatt, A., and Kamens, R. M.: Oxidant generation and toxicity enhancement of aged-diesel exhaust, Atmos. Environ., 43, 1037-1042, http://dx.doi.org/10.1016/j.atmosenv.2008.11.018, 2009.
Li, Q., Shang, J., and Zhu, T.: Physicochemical characteristics and toxic effects of ozone-oxidized black carbon particles, Atmos. Environ., 81, 68-75, http://dx.doi.org/10.1016/j.atmosenv.2013.08.043, 2013.
Li, Q., Shang, J., Liu, J., Xu, W., Feng, X., Li, R., and Zhu, T.: Physicochemical characteristics, oxidative capacities and cytotoxicities of sulfate-coated, 1,4-NQ-coated and ozone-aged black carbon particles, Atmos. Res., 153, 535-542, http://dx.doi.org/10.1016/j.atmosres.2014.10.005, 2015.
Li, R. B., Guiney, L. M., Chang, C. H., Mansukhani, N. D., Ji, Z. X., Wang, X., Liao, Y. P., Jiang, W., Sun, B. B., Hersam, M. C., Nel, A. E., and Xia, T.: Surface oxidation of graphene oxide determines membrane damage, lipid peroxidation, and cytotoxicity in macrophages in a pulmonary toxicity model, ACS Nano, 12, 1390-1402, 10.1021/acsnano.7b07737, 2018.
Liu, Q., Baumgartner, J., Zhang, Y., Liu, Y., Sun, Y., and Zhang, M.: Oxidative potential and inflammatory impacts of source apportioned ambient air pollution in beijing, Environ. Sci. Technol., 48, 12920-12929, 10.1021/es5029876, 2014a.
Liu, Y., Liu, C., Ma, J., Ma, Q., and He, H.: Structural and hygroscopic changes of soot during heterogeneous reaction with O_3, Phys. Chem. Chem. Phys., 12, 10896-10903, 2010.
Liu, Y., Ai, K., and Lu, L.: Polydopamine and its derivative materials: Synthesis and promising applications in energy, environmental, and biomedical fields, Chem. Rev., 114, 5057-5115, 10.1021/cr400407a, 2014b.
Liu, Y., Liggio, J., Li, S.-M., Breznan, D., Vincent, R., Thomson, E. M., Kumarathasan, P., Das, D., Abbatt, J., Antiñolo, M., and Russell, L.: Chemical and toxicological evolution of carbon nanotubes

718 during atmospherically relevant aging processes, Environ. Sci. Technol., 49, 2806-2814,
719 10.1021/es505298d, 2015.
720 Long, C. M., Nascarella, M. A., and Valberg, P. A.: Carbon black vs. black carbon and other airborne
721 materials containing elemental carbon: Physical and chemical distinctions, Environ. Pollut., 181, 271-
722 286, http://dx.doi.org/10.1016/j.envpol.2013.06.009, 2013.
723 Maruyama, T.: Current status of single-walled carbon nanotube synthesis from metal catalysts by
724 chemical vapor deposition, Mat. Exp., 8, 1-20, 10.1166/mex.2018.1407, 2018.
725 Mawhinney, D. B., Naumenko, V., Kuznetsova, A., Yates, J. T., Liu, J., and Smalley, R. E.: Infrared
726 spectral evidence for the etching of carbon nanotubes: Ozone oxidation at 298 K, J. Am. Chem. Soc.,
727 122, 2383-2384, 10.1021/ja994094s, 2000.
728 McWhinney, R. D., Badali, K., Liggio, J., Li, S.-M., and Abbatt, J. P. D.: Filterable redox cycling activity:
729 A comparison between diesel exhaust particles and secondary organic aerosol constituents, Environ. Sci.
730 Technol., 47, 3362-3369, 10.1021/es304676x, 2013a.
731 McWhinney, R. D., Zhou, S., and Abbatt, J. P. D.: Naphthalene SOA: redox activity and naphthoquinone
732 gas–particle partitioning, Atmos. Chem. Phys., 13, 9731-9744, 10.5194/acp-13-9731-2013, 2013b.
733 Muckenhuber, H., and Grothe, H.: The heterogeneous reaction between soot and NO_2 at elevated
734 temperature, Carbon 44, 546-559, 2006.
735 Nel, A., Xia, T., Määdler, L., and Li, N.: Toxic potential of materials at the nanolevel., Science, 311, 622-
736 627, 2006.
737 Nienow, A. M., and Roberts, J. T.: Heterogeneos chemsitry of carbon aerosols, Annu. Rev. Phys. Chem.,
738 57, 105-128, 2006.
739 Niranjan, R., and Thakur, A. K.: The toxicological mechanisms of environmental soot (black carbon) and
740 carbon black: focus on oxidative stress and inflammatory pathways, Front. Immunol., 8, 20,
741 10.3389/fimmu.2017.00763, 2017.
742 Parant, H., Muller, G., Le Mercier, T., Tarascon, J. M., Poulin, P., and Colin, A.: Flowing suspensions of
743 carbon black with high electronic conductivity for flow applications: Comparison between carbons black
744 and exhibition of specific aggregation of carbon particles, Carbon, 119, 10-20,
745 10.1016/j.carbon.2017.04.014, 2017.
746 Peebles, B. C., Dutta, P. K., Waldman, W. J., Villamena, F. A., Nash, K., Severance, M., and Nagy, A.:
747 Physicochemical and toxicological properties of commercial carbon blacks modified by reaction with
748 ozone, Environ. Sci. Technol., 45, 10668-10675, 2011.
749 Sanders, I. J., and Peeten, T. L.: Carbon black: Production, properties and uses, edited by: Technologies,
750 Nova Science Publishers, UK, 293 pp., 2011.
751 Schuster, M. E., Hävecker, M., Arrigo, R., Blume, R., Knauer, M., Ivleva, N. P., Su, D. S., Niessner, R.,
752 and Schlögl, R.: Surface sensitive study to determine the reactivity of soot with the focus on the european
753 emission standards IV and VI, J. Phys. Chem. A., 115, 2568-2580, 10.1021/jp1088417, 2011.
754 Shvedova, A. A., Pietroiusti, A., Fadeel, B., and Kagan, V. E.: Mechanisms of carbon nanotube-induced
755 toxicity: Focus on oxidative stress, Toxicol. Appl. Pharmacol., 261, 121-133, 2012.
756 Simmons, J. M., Nichols, B. M., Baker, S. E., Marcus, M. S., Castellini, O. M., Lee, C. S., Hamers, R.
757 J., and Eriksson, M. A.: Effect of ozone oxidation on single-walled carbon nanotubes, J. Phys. Chem. B,
758 110, 7113-7118, 10.1021/jp0548422, 2006.
759 Somiya, S.: Handbook of Advanced Ceramics, 2nd ed., Academic Press, 2013.
760 Tiwari, A. J., and Marr, L. C.: The role of atmospheric transformations in determing envrionmental
761 impacts of carbonaceous nanoparticles, J. Environ. Qual., 39, 1883-1895, 2010.

762 Truong, H., Lomnicki, S., and Dellinger, B.: Potential for misidentification of environmentally persistent
763 free radicals as molecular pollutants in particulate matter, Environ. Sci. Technol., 44, 1933-1939,
764 10.1021/es902648t, 2010.
765 Wang, B., Li, K., Jin, W., Lu, Y., Zhang, Y., Shen, G., Wang, R., Shen, H., Li, W., Huang, Y., Zhang, Y.,
766 Wang, X., Li, X., Liu, W., Cao, H., and Tao, S.: Properties and inflammatory effects of various size
767 fractions of ambient particulate matter from beijing on A549 and J774A.1 Cells, Environ. Sci. Technol.,
768 47, 10583-10590, 10.1021/es401394g, 2013.
769 WHO: World Health Organization. Health effects of particulate matter: Policy implications for countries
770 in eastern Europe, Caucasus and central Asia, 2013.
771 Xia, T., Kovochich, M., Brant, J., Hotze, M., Sempf, J., Oberley, T., Sioutas, C., Yeh, J. I., Wiesner, M.
772 R., and Nel, A. E.: Comparison of the abilities of ambient and manufactured nanoparticles to induce
773 cellular toxicity according to an oxidative stress paradigm, Nano Lett., 6, 1794-1807, 10.1021/nl061025k,
774 2006.
775 Yim, W. L., and Johnson, J. K.: Ozone oxidation of single walled carbon nanotubes from density
776 functional theory, J. Phys. Chem. C, 113, 17636-17642, 10.1021/jp908089c, 2009.
777 Zhang, B., Wei, P., Zhou, Z., and Wei, T.: Interactions of graphene with mammalian cells: Molecular
778 mechanisms and biomedical insights, Ad. Drug Del. Rev., 105, 145-162,
779 https://doi.org/10.1016/j.addr.2016.08.009, 2016.
780 Zhang, X., Wang, S., Xu, L., Feng, L., Ji, Y., Tao, L., Li, S., and Wei, Y.: Biocompatible polydopamine
781 fluorescent organic nanoparticles: facile preparation and cell imaging, Nanoscale, 4, 5581-5584,
782 10.1039/c2nr31281f, 2012.

783

784

Figure captions

Figure 1. DTT decay rates of several black carbon materials compared with literature results (Li et al., 2013;Charrier and Anastasio, 2012;Liu et al., 2014a;Li et al., 2015;Liu et al., 2015;Holder et al., 2012;Antinolo et al., 2015).

Figure 2. Cytotoxicity of (A) SB4A, (B) graphene, (C) graphene oxide, (D) SWCNT, (E) SWCNT-OH and (F) SWCNT-COOH toward murine J774 cell line. The stars mean the difference is significant at 0.05 level for a certain dose of carbon nanomaterials compared with the corresponding blank experiments.

Figure 3. (A) Thermo gravity curves of carbon nanomaterials in nitrogen gas flow; (B) the corresponding differential thermal analysis curves. The insert graph shows the weight loss due to desorption of organics.

Figure 4. XPS spectra of carbon nanomaterials. (A)-(F) are O1s spectra and (G)-(L) are C1s spectra for SB4A, graphene, graphene oxide, SWCNT, SWCNT-OH and SWCNT-COOH, respectively.

Figure 5. (A) Distribution of oxygen containing species on the tested carbon nanomaterials; (B) comparison of oxygen-containing species and (C) DTT decay rate between graphene oxide and other carbon nanomaterials.

Figure 6. DTT decay rate for graphene oxide and thermally treated graphene oxide in N_2 flow at 200 °C.

805 **Figures**

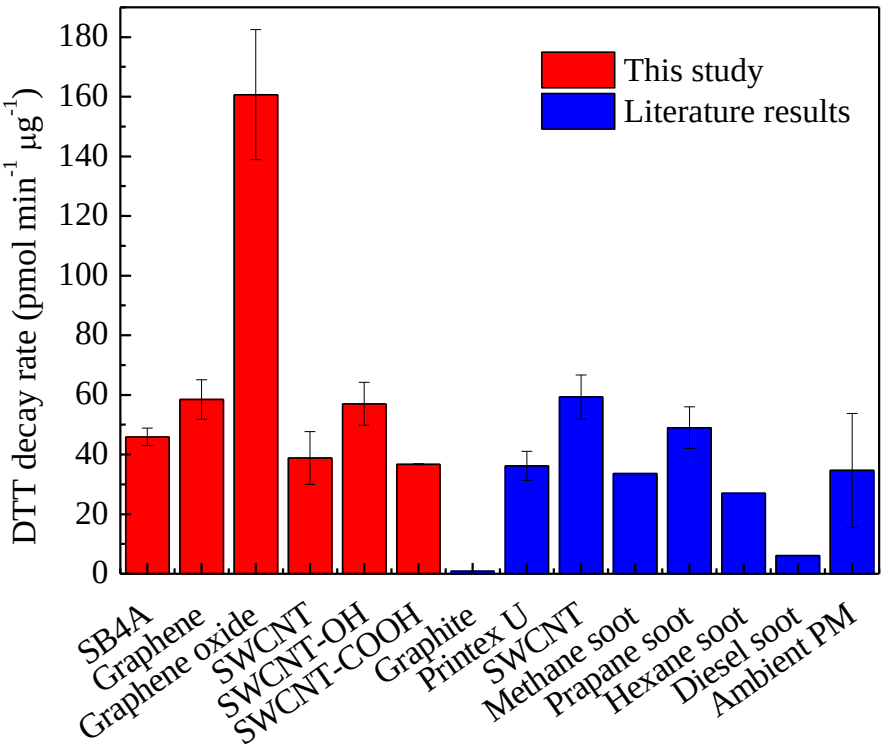

806

807 Fig. 1

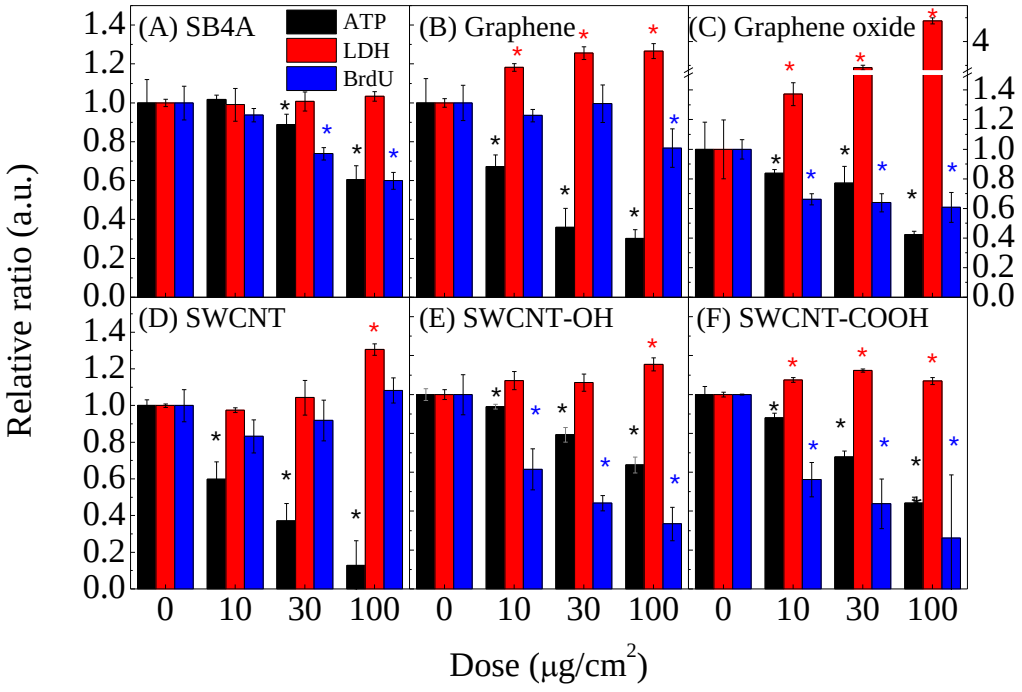

808

809 Fig. 2

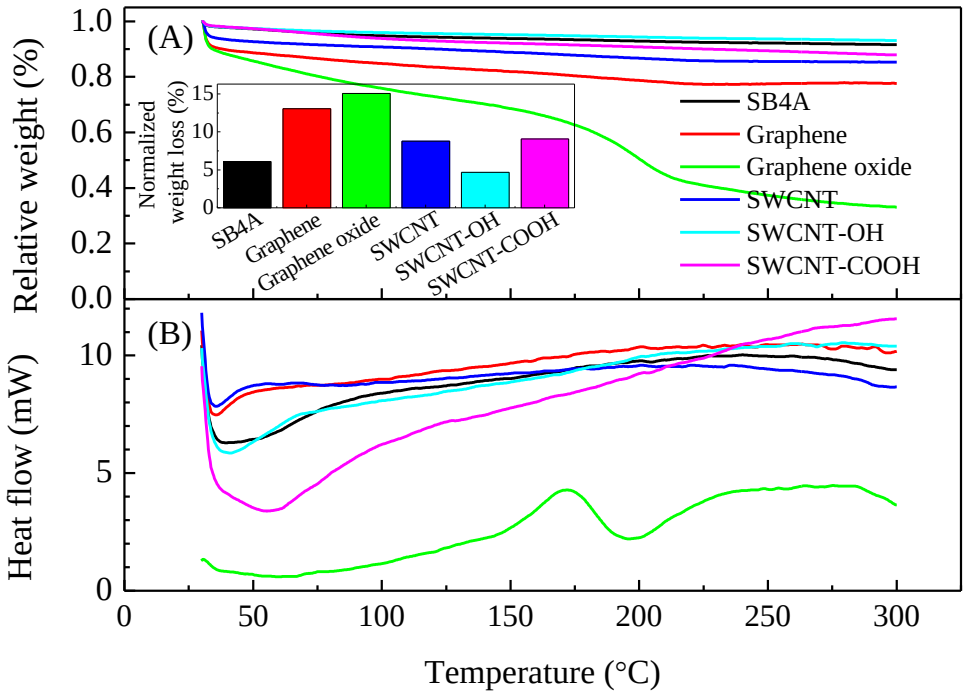
(A)
(B)
Relative weight (%)
Heat flow (mW)
Temperature (°C)
Normalized weight loss (%)
SB4A
Graphene
Graphene oxide
SWCNT
SWCNT-OH
SWCNT-COOH

Fig. 3.

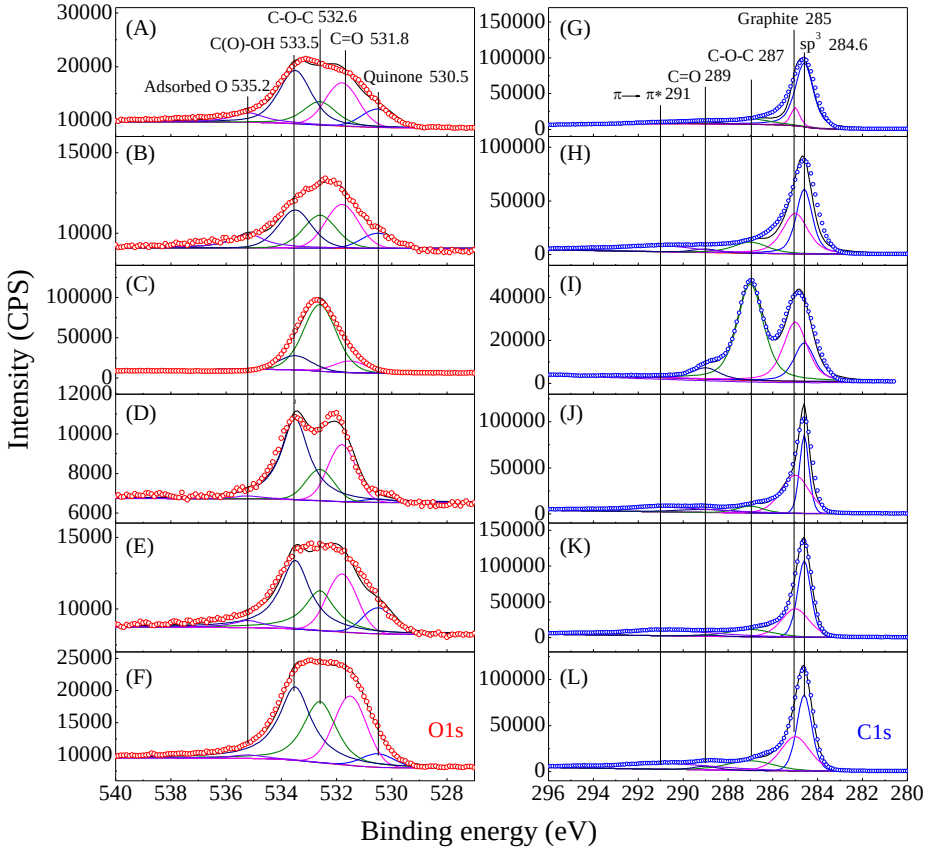
(A)
C-O-C 532.6
C(O)-OH 533.5
C=O 531.8
Adsorbed O 535.2
Quinone 530.5
(G)
Graphite 285
C-O-C 287
sp3 284.6
C=O 289
π—→π* 291
O1s
C1s
Intensity (CPS)
Binding energy (eV)

813 Fig. 4.

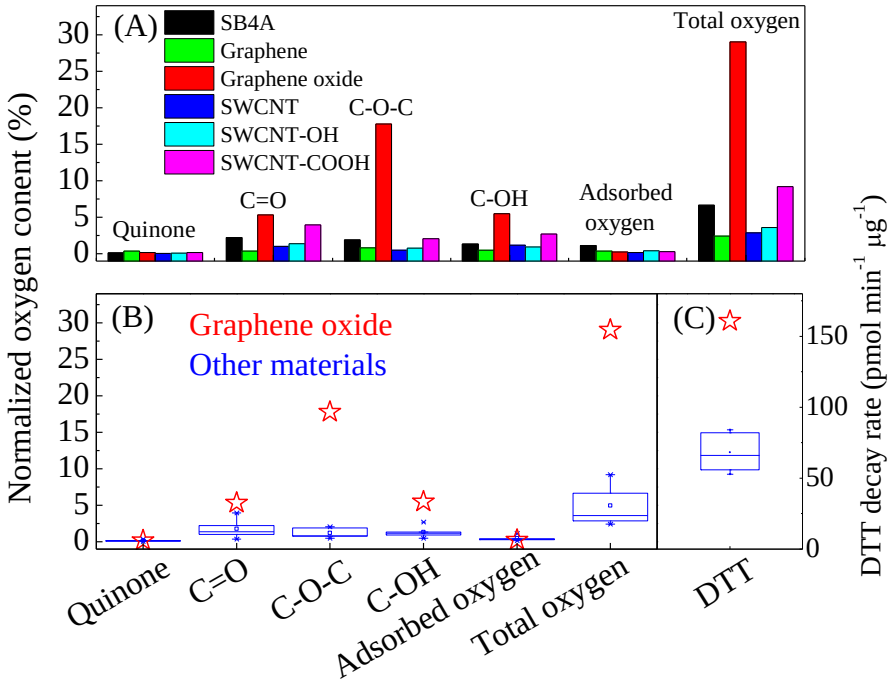

814

815 Fig. 5.

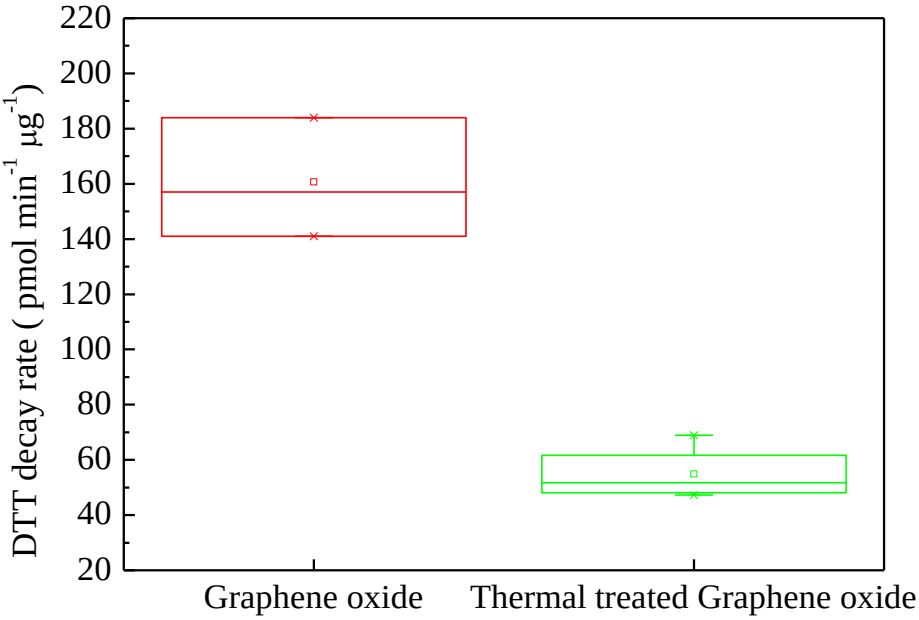

816

817 Figure 6.

818